Faithful Quantum Teleportation via a Nanophotonic Nonlinear Bell State Analyzer

Joshua Akin,[1,2] Yunlei Zhao,[1,2] Paul G. Kwiat,[2,3] Elizabeth A. Goldschmidt,[2,3] and Kejie Fang[1,2,*]
[1]Holonyak Micro and Nanotechnology Laboratory and Department of Electrical and Computer Engineering, University of Illinois at Urbana-Champaign, Urbana, Illinois 61801, USA
[2]Illinois Quantum Information Science and Technology Center, University of Illinois at Urbana-Champaign, Urbana, Illinois 61801, USA
[3]Department of Physics, University of Illinois at Urbana-Champaign, Urbana, Illinois 61801, USA

(Received 22 November 2024; accepted 24 March 2025; published 22 April 2025)

Quantum networking protocols, including quantum teleportation and entanglement swapping, use linear-optical Bell state measurements for heralding the distribution and transfer of quantum information. However, a linear-optical Bell state measurement requires identical photons and is susceptible to errors caused by multiphoton emission, fundamentally limiting the efficiency and fidelity of quantum networking protocols. Here we show a nonlinear Bell state analyzer for time-bin encoded photons based on a nanophotonic cavity with a sum-frequency generation efficiency of 4×10^{-5} to filter multiphoton emissions, and utilize it for faithful quantum teleportation involving spectrally distinct photons with fidelities $\geq 94\%$ down to the single-photon level. Our result demonstrates that nonlinear-optical entangling operations, empowered by our efficient nanophotonics platform, can realize faithful quantum information protocols without requiring identical photons and without the fundamental limit on the fidelity of a Bell state measurement imposed by linear optics, which facilitates the realization of practical quantum networks.

DOI: 10.1103/PhysRevLett.134.160802

Quantum information is unique because the linearity of quantum mechanics prevents the cloning of quantum states [1]. This is advantageous for information security but a drawback overall, as it prevents the amplification of quantum signals to counteract loss over transmission channels. Quantum teleportation can circumvent this issue by indirectly transferring quantum information using quantum entanglement and a classical communication channel [2], without the original quantum particle needing to traverse the entire distance. The concept can be extended to establish entanglement between distant quantum nodes via entanglement swapping [3]. With a dual network of distributed entanglement and classical communication, it is possible to send quantum information over arbitrary distances [4,5]. Since the first experimental demonstration of quantum teleportation [6], tremendous advances have been made toward realizing a practical quantum network [7–10].

Most quantum networking protocols, including quantum teleportation and entanglement swapping, rely on linear-optical Bell state measurements (LO-BSMs) by interfering two identical photons at a beam splitter to herald the distribution and transfer of quantum information. However, a LO-BSM requires the two input photons to be identical, leading to false heralds in the presence of multiphoton emission [11,12], which is ubiquitous among probabilistic quantum light sources and many quantum emitters. This flaw fundamentally limits the efficiency and fidelity of entanglement distribution [5,13]. For instance, quantum teleportation using heralded single-photon sources needs substantial attenuation of the source to achieve a high fidelity without postselection [12], i.e., without detection of the teleported photon. The latter is necessary for the subsequent manipulation of the teleported photon. Moreover, for entanglement swapping using nonlinear optics-based entangled photon sources and LO-BSMs, the non-postselected fidelity is bounded by $\mathcal{F} \leq 1/3$ [14]. The requirement that the input photons are identical leads to another fundamental constraint on LO-BSMs as any nonidenticality reduces the fidelity of the protocol. However, in an actual quantum network with independently produced single and entangled photons traversing dispersive or otherwise unstable channels, it is a major challenge to ensure perfect indistinguishability. Real-world demonstrations of transferring quantum information or distributing entanglement over even a small number of quantum nodes suffer from substantial errors due to this constraint [10,16–18].

In this Letter, we demonstrate a nonlinear Bell state analyzer and utilize it for quantum teleportation of time-bin encoded qubits involving spectrally distinct photons. In contrast to a LO-BSM, a nonlinear Bell state analyzer leverages the sum-frequency generation (SFG) between nondegenerate photons to filter multiphoton emissions

*Contact author: kfang3@illinois.edu

from either source, resulting in faithful quantum teleportation and entanglement swapping without the fidelity-efficiency trade-off [19]. Nevertheless, the efficiency of the nonlinear Bell state analyzer is fundamentally limited by the efficiency of SFG. Prior attempts to use SFG for quantum information protocols, including high-dimensional teleportation [20,21], were limited by the low SFG efficiency of bulk nonlinear crystals and waveguides [19–26], requiring the use of intense optical fields for the SFG. As a result, demonstrating the quantum coherence of the nonlinear interaction at the few- and single-photon levels has proven elusive. Our demonstration capitalizes on an $In_{0.5}Ga_{0.5}P$ nanophotonic cavity with a SFG efficiency of 4×10^{-5}, transcending the limit of bulk nonlinear crystals and waveguides by several orders of magnitude. With the nanophotonic nonlinear Bell state analyzer, we achieve an average fidelity $\geq 94\%$ for the SFG-heralded quantum teleportation of time-bin encoded photonic states down to the single-photon level and validate the robustness of this scheme against multiphoton emission and over long optical fibers.

For SFG-heralded quantum teleportation (Fig. 1), a nonlinear optical element supports three-wave mixing between Alice's photon and one photon of the entanglement source to generate a photon at the sum of the two frequencies. This implements a nonlinear-optical (NLO) BSM when the SFG photon is measured in a basis that encodes the Bell states of the two incoming photonic qubits. The detection of the SFG photon heralds the teleportation of the quantum state of Alice's photon to Bob's photon, up to a single-qubit rotation that depends on the outcome of the measurement of the SFG photon. Because the SFG process is only phase-matched for nondegenerate photons, multiphoton emissions from the same source cannot be up-converted, thus eliminating the vacuum and a portion of uncorrelated photons in the heralded signal. The fidelity of the SFG-heralded teleportation, whether or not it is postselected, is given by [14]

$$\mathcal{F} = \left(\frac{1+\sqrt{1-4p_{si}}}{2}\right)^2, \tag{1}$$

where p_{si} is the single-photon-pair probability of the entanglement source. In deriving Eq. (1), we assumed thermal number statistics of the photon pair, as is typical for nonlinear optics-based entangled photon sources [27], leading to $p_{si} \leq \frac{1}{4}$, while Alice is an arbitrary pure state. The fidelity exceeds the classical bound of 2/3 even for relatively large $p_{si}(\leq 0.15)$, corresponding to a nonnegligible multipair probability, and it is independent of Alice's photon number. This indicates that a true single-photon source is not necessary for the nonlinear Bell state analyzer and sources can be driven more efficiently with less reduction in the fidelity of protocols. The nonlinear Bell state analyzer also avoids the stringent requirement of quantum interference of identical photons, as the two input photons now only need to satisfy the phase-matching condition of SFG—deviating from this condition only affects the efficiency but not the fidelity of the protocol, i.e., the phase-matching condition filters the variations of input photons. Beyond quantum teleportation, nonlinear Bell state analyzers with even moderate SFG efficiency can enable faithful heralded entanglement swapping [14,19]—a critical protocol for quantum repeaters. Moreover, nonlinear Bell state analyzers can be used to establish entanglement between heterogeneous or distinguishable quantum emitters without the need of wavelength conversion or compensation.

The nonlinear Bell state analyzer in our experiment is implemented for time-bin encoded photons, which are robust for quantum information transmission in optical fibers [28]. Alice's photon is prepared in a superposition state of the early and late time bins, $|\psi_A\rangle = \alpha|e\rangle_A + \beta|l\rangle_A$, while the entangled photon source generates a photon pair in the Bell state $|\Phi^+\rangle_{si} = (1/\sqrt{2})(|e\rangle_s|e\rangle_i + |l\rangle_s|l\rangle_i)$. The joint state of the three photons can be expressed as

$$\begin{aligned}&|\psi_A\rangle \otimes |\Phi^+\rangle_{si} \\ &= \frac{1}{2}(|\Phi^+\rangle_{As}(\alpha|e\rangle_i + \beta|l\rangle_i) + |\Phi^-\rangle_{As}(\alpha|e\rangle_i - \beta|l\rangle_i) \\ &\quad + |\Psi^+\rangle_{As}(\alpha|l\rangle_i + \beta|e\rangle_i) + |\Psi^+\rangle_{As}(\alpha|l\rangle_i - \beta|e\rangle_i)),\end{aligned} \tag{2}$$

where $|\Phi^\pm\rangle_{As} = (1/\sqrt{2})(|e\rangle_A|e\rangle_s \pm |l\rangle_A|l\rangle_s)$ and $|\Psi^\pm\rangle_{As} = (1/\sqrt{2})(|e\rangle_A|l\rangle_s \pm |l\rangle_A|e\rangle_s)$ are the four Bell states. SFG can happen in the nonlinear element when both Alice's photon and signal photon are in the same time bin, i.e., in the case of Bell states $|\Phi^\pm\rangle_{As}$. Conditioned on SFG, which occurs with a small probability p_{SFG}, the joint state of the initial three photons becomes

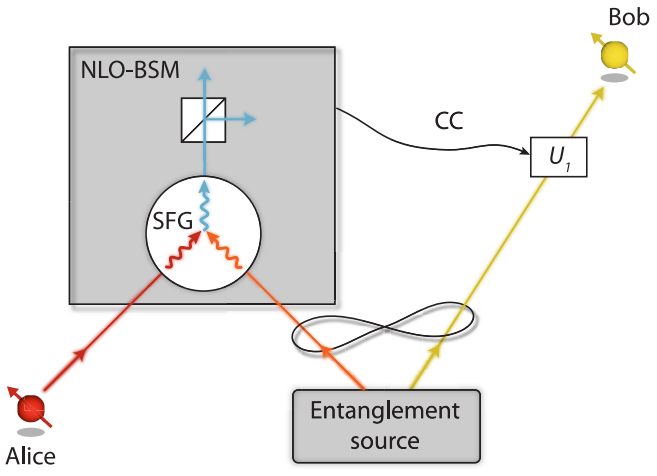

FIG. 1. Nonlinear Bell state analyzer. A schematic of a NLO-BSM that leverages the SFG process being used for quantum teleportation involving spectrally distinct photons. CC: classical communication.

$$|\psi_A\rangle \otimes |\Phi^+\rangle_{si} \xrightarrow{\text{SFG}} \frac{1}{2}(|\Sigma^+\rangle(\alpha|e\rangle_i + \beta e^{-i\varphi_\Sigma}|l\rangle_i) + |\Sigma^-\rangle(\alpha|e\rangle_i - \beta e^{-i\varphi_\Sigma}|l\rangle_i)), \quad (3)$$

where $|\Sigma^\pm\rangle = (1/\sqrt{2})(|e\rangle_\Sigma \pm e^{i\varphi_\Sigma}|l\rangle_\Sigma)$ are the two orthogonal SFG photon states corresponding to Bell states $|\Phi^\pm\rangle_{As}$ and phase φ_Σ is introduced during the projection measurement of the SFG photon. Note a unitary transformation of Bob's photon is necessary even for $\varphi_\Sigma = 0$, if the SFG photon is projected to $|\Sigma^-\rangle$. A second nonlinear element and delay lines can be introduced to enable SFG between $|e\rangle$ and $|l\rangle$, allowing the other two Bell states $|\Psi^\pm\rangle_{As}$ to also be distinguished and thus realizing a complete Bell state analyzer [14], which is impossible with passive linear optics and unentangled ancillary photons [29–31]. By measuring the SFG photon in the $|\Sigma^\pm\rangle$ basis, the idler photon is projected to a single-photon state, which differs from the original Alice's photon up to a single-qubit rotation.

Our nonlinear Bell state analyzer exploits a $\chi^{(2)}$ nonlinear microring resonator made from thin-film $In_{0.5}Ga_{0.5}P$ (Fig. 2 inset), which possesses a very large second-order nonlinearity, low optical losses, and wavelength-scale optical confinement [32] to bolster the efficiency of the SFG process (Appendix A). The schematic of the experimental setup is depicted in Fig. 2. The nonlinear Bell state analyzer is located in one laboratory and the rest of the setup is in another laboratory. Alice's time-bin state is prepared from an attenuated laser pulse, which passes through an unbalanced Mach-Zehnder interferometer (MZI) made from glass integrated photonic circuits to form the early and late time bins with a delay of $\tau = 1$ ns. The optical pulse is created by intensity modulation of a continuous-wave laser. Attenuated laser beams can be applied to decoy state protocols developed through quantum cryptography [33] and quantum fingerprinting [34], and are widely used in quantum teleportation experiments [18,35–37]. The frequency of Alice's pulse matches mode a of the microring resonator with a pulse width of 330 ps and a repetition rate of 250 MHz. The phase difference φ_A between the early and late time bins is controlled and stabilized via the temperature of the glass MZI. The microwave pulse that drives the intensity modulator for Alice's pulses serves as the clock for the time-bin pulse sequence. The entangled photon pair is generated via spontaneous parametric down-conversion (SPDC) in a periodically poled $LiNbO_3$ waveguide pumped by a continuous-wave laser at the pump wavelength $\lambda_p = 771.921$ nm. Both Alice's laser and the SPDC pump laser are stabilized by a wave meter but are not phase locked to each other.

The SPDC photon pairs generated by a continuous-wave pump are in a time-frequency entangled state. However, only those signal photons that are time matched with the time bins defined by Alice's pulses and frequency-matched with mode b of the microring resonator can interact with Alice's photon to generate the SFG photon. Consequently, the frequency- and time-matched signal

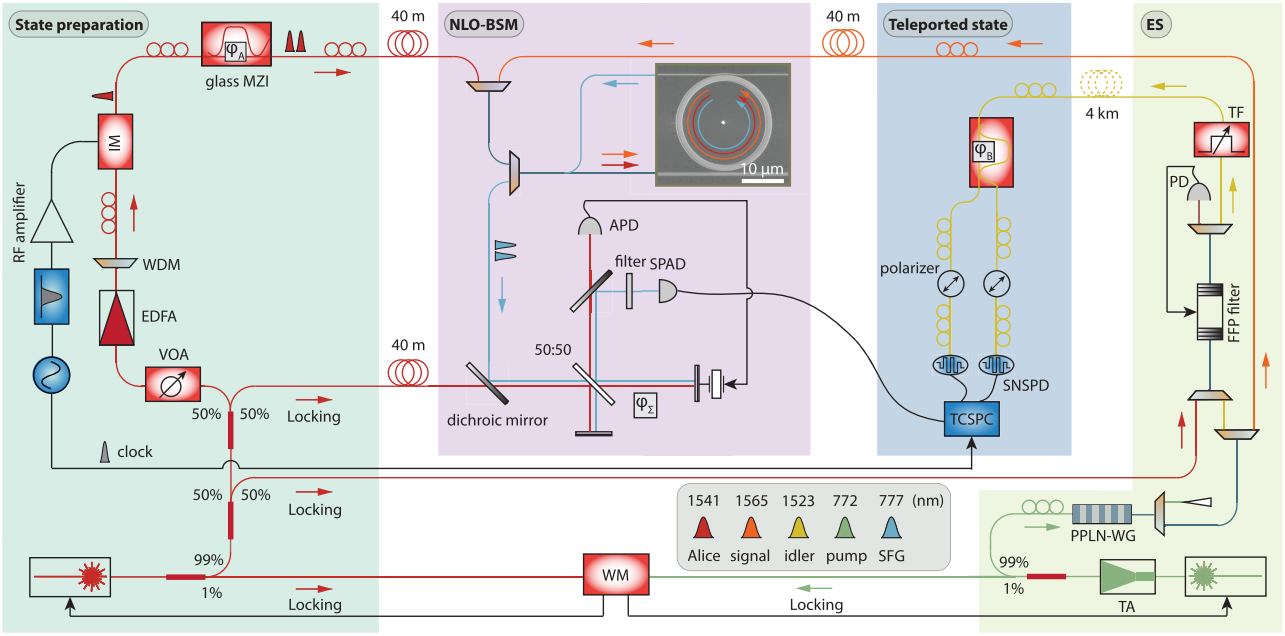

FIG. 2. SFG nanophotonic cavity and quantum teleportation setup. Schematic of the experimental setup. A scanning electron microscope image of the $In_{0.5}Ga_{0.5}P$ nonlinear nanophotonic cavity is shown. ES: entanglement source. VOA: variable optical attenuator. EDFA: erbium-doped fiber amplifier. WDM: wavelength division-multiplexer. IM: intensity modulator. MZI: Mach-Zehnder interferometer. PPLN-WG: periodically poled lithium niobate waveguide. FFP filter: fiber Fabry-Perot filter. TF: tunable filter. APD: avalanche photodetector. SPAD: single-photon avalanche diode detector. SNSPD: superconducting nanowire single-photon detector. TCSPC: time-correlated single-photon counting module. WM: wavelength meter. TA: tapered amplifier.

and idler time-bin qubits are gated by Alice's pulses to form the Bell state $|\Phi^+\rangle_{si}$. The average number of signal photons in the resonator for each signal time-bin qubit is $\langle n_b\rangle = 5.4\times10^{-3} \ll 1$, and thus there is at most one photon in Alice's time-bin state that is converted to a SFG photon. The idler photon entangled with the signal photon is wavelength selected by a tunable fiber Fabry-Perot filter with a bandwidth similar to the microring resonator. To herald the quantum teleportation, the SFG time-bin qubit is projected to the $|\Sigma^\pm\rangle$ states using a free-space unbalanced Michelson interferometer whose time delay matches that of the time-bin qubit and whose phase delay φ_Σ is controlled by a motorized stage. Both the fiber Fabry-Perot filter and the Michelson interferometer are stabilized to Alice's laser. Quantum state tomography of Bob's teleported time-bin qubit is performed using a glass integrated photonic circuit MZI with a tunable phase delay φ_B to project Bob's qubit to the three axes of the Bloch sphere, from which the density matrix can be constructed. More information about the setup and measurement details is provided in [14].

Figure 3(a) shows the measured on-chip SFG rate as a function of the mode a cavity photon number, $\langle n_a\rangle = P_a/(\hbar\omega_a\kappa_a)$, down to the single-photon level, with the mode b cavity photon number fixed at $\langle n_b\rangle = 5.4\times10^{-3}$. We inferred a SFG efficiency $\eta_{\rm SFG} \equiv P_{\rm SFG}/(P_aP_b) = 4.4\times10^4\%/{\rm W}$, where all the powers are the on-chip power, and the corresponding single-photon SFG probability $p_{\rm SFG} = 4g^2/\bar{\kappa}_{a,b}\kappa_c \approx 4\times10^{-5}$, where κ_k is the dissipation rate of mode k [14]. This marks an improvement over prior nonlinear waveguides by three orders of magnitude [23–26]. Next we measured the entanglement between the time-bin encoded SFG and idler photons. The interferometers are stabilized to limit phase variances to $\Delta\varphi_{A,B} = 1.1\times10^{-3}\pi$ and $\Delta\varphi_\Sigma = 2.4\times10^{-3}\pi$ over one hour [14]. After passing through the unbalanced interferometers, the time-bin encoded SFG and idler photons appear in three time bins, where the middle time bin contains a temporally overlapped superposition of the original early and late states. From Eq. (3), the coincidence

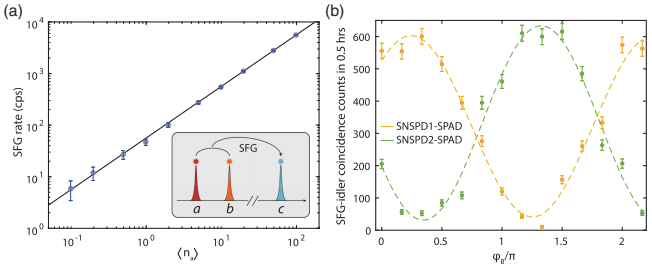

FIG. 3. Entanglement between time-bin encoded SFG and idler photons. (a) On-chip SFG rate versus cavity photon number $\langle n_a\rangle$, with $\langle n_b\rangle = 5.4\times10^{-3}$. The line is a linear fit. (b) Coincidences between time-bin encoded SFG and idler photons detected by the SPAD and SNSPDs, respectively. SFG cavity photon number $\langle n_\Sigma\rangle \approx 10^{-5}$. Statistical error bars are one standard deviation.

counts between the middle-bin SFG photon $|\Sigma^+\rangle = (1/\sqrt{2})(|e\rangle_\Sigma + e^{i\varphi_\Sigma}|l\rangle_\Sigma)$ (detected in a single output port with a SPAD) and middle-bin idler photon $|\psi_B\rangle = (1/\sqrt{2})(|e\rangle_i \pm e^{i\varphi_B}|l\rangle_i)$, where the $\pm$ depends on which output port SNSPD detects the photon, are given by

$$C_{\Sigma|B} = N_0[1 \pm \cos(\varphi_A - \varphi_\Sigma - \varphi_B)], \tag{4}$$

where Alice's photon is in state $|\psi_A\rangle = (1/\sqrt{2})(|e\rangle_A + e^{i\varphi_A}|l\rangle_A)$. Figure 3(b) shows the measured SFG-idler coincidence fringes (after subtraction of the accidental coincidences) for the SFG cavity photon number $\langle n_\Sigma\rangle \approx 10^{-5}$, by varying φ_B and fixing $\varphi_{A,\Sigma}$. The visibility of the coincidence fringe is $\mathcal{V} = 90.5\%$, which exceeds the Clauser-Horne limit of $(1/\sqrt{2}) \approx 70.7\%$ [38] and verifies the entanglement between the SFG and idler time-bin qubits. The visibility of the coincidence fringe is primarily limited by the imperfect visibility of individual interferometers [14].

We then used the nonlinear Bell state analyzer for teleportation of different Alice states $|e\rangle$, $|l\rangle$, $|+\rangle$, $|-\rangle$, $|R\rangle$, and $|L\rangle$, which are prepared by varying φ_A or by removing Alice's MZI in the case of $|e\rangle$ and $|l\rangle$. The teleportation is heralded by the detection of the SFG photon in the $|\Sigma^+\rangle$ state. Quantum state tomography of the teleported state is performed via the time-resolved detection of idler photons conditioned on the detection of $|\Sigma^+\rangle$ state, and the density matrix of the teleported state is constructed

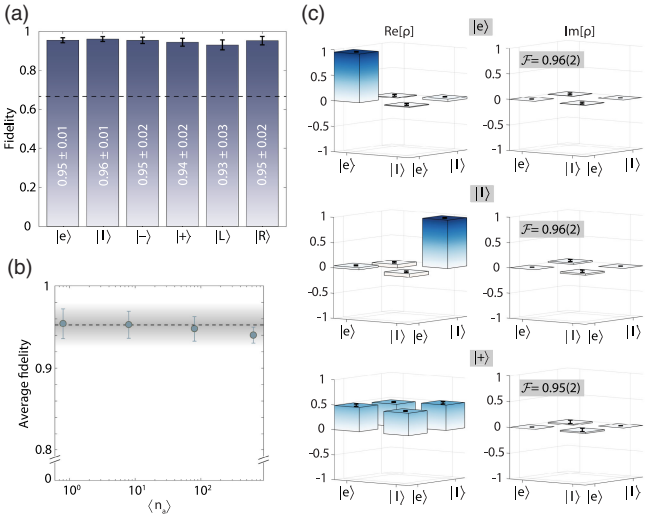

FIG. 4. Experimental results for SFG-heralded quantum teleportation. (a) A summary of the teleportation fidelities for the states $|e\rangle$, $|l\rangle$, $|-\rangle$, $|+\rangle$, $|L\rangle$, and $|R\rangle$. $\langle n_a\rangle = 80$. Dashed line indicates the classical bound of $\frac{2}{3}$. Error bars, 1 s.d., deduced from propagated Poissonian counting statistics of the raw detection events and interferometer phase fluctuations. (b) Average fidelity of teleported states $|e\rangle$, $|l\rangle$, and $|+\rangle$ for various $\langle n_a\rangle$. Dashed line and shaded area represent the calculated fidelity $\mathcal{F} = (1+\mathcal{V})/2$ and variance $\Delta\mathcal{F} = \Delta\mathcal{V}/2$. (c) Density matrix and fidelity of teleported states $|e\rangle$, $|l\rangle$, and $|+\rangle$ for $\langle n_a\rangle = 0.8$.

using maximum likelihood estimation [14,39]. The fidelity of the six states for a cavity photon number of Alice $\langle n_a \rangle = 80$ is summarized in Fig. 4(a). The average fidelity of the six states, $\bar{\mathcal{F}} = 94.4 \pm 1.8\%$, is well above the classical limit of $\frac{2}{3}$. We also varied the cavity photon number of Alice and performed quantum teleportation of $|e\rangle$, $|l\rangle$, $|+\rangle$ states down to the single-photon level. The average fidelity of the three states versus cavity photon number $\langle n_a \rangle$ is shown in Fig. 4(b) and the density matrix of the teleported $|e\rangle$, $|l\rangle$, $|+\rangle$ states for $\langle n_a \rangle = 0.8$ is displayed in Fig. 4(c) (see Ref. [14] for the density matrix and fidelity of all measured states). The high fidelity ($\geq 94\%$) across all the measured cavity photon numbers proves that the nonlinear Bell state analyzer is immune to multiphoton-driven errors, while, in contrast, a LO-BSM is unfeasible in the high-photon-number regime [37]. We also performed SFG-heralded quantum teleportation over long distances using a 4 km-long fiber spool inserted between the entangled photon source and Bob. The fidelity drops slightly to $\bar{\mathcal{F}} = 90.5 \pm 1.6\%$, mainly because the visibility of the glass integrated photonic circuit MZI is polarization sensitive and the polarization drifts in the long fiber during the integration time.

In summary, we have demonstrated a nonlinear Bell state analyzer and applied it for faithful quantum teleportation of time-bin encoded photonic states down to the single-photon level. Key to this demonstration is a nanophotonic cavity with a single-photon SFG probability (4×10^{-5}) three orders of magnitude greater than prior nonlinear waveguides [23–26]. Using state-of-the-art $In_{0.5}Ga_{0.5}P$ microring resonators with a nonlinearity-to-loss ratio (g/κ) of a few percent [32,40], we expect to be able to achieve SFG probability ($p_{\mathrm{SFG}} \sim 4(g/\kappa)^2$) on the order of 10^{-3}. Beyond quantum teleportation, the nonlinear Bell state analyzer can enable quantum networking protocols, including heralded entanglement swapping [19,41], with a much higher fidelity than linear-optical schemes (Appendix B and [14]). Given that quantum light sources can be driven more efficiently when using the nonlinear Bell state analyzer, since it directly projects out unwanted multipair noise events, our approach should already achieve an entanglement rate higher than or on par with using LO-BSM in some practical scenarios (Appendix B and [14]). Furthermore, teleportation of high-dimensional quantum information via nonlinear interactions is also possible, following the proof-of-principle demonstrations with intense optical fields [20,21].

Acknowledgments—We thank Liang Jiang and Eric Chitambar for their discussions. This work is supported by US National Science Foundation under Grant No. 2223192 and QLCI-HQAN (Grant No. 2016136) and U.S. Department of Energy Office of Science National Quantum Information Science Research Centers.

K. F., E. A. G., P. G. K. proposed the experiment. J. A. fabricated the device. J. A., Y. Z. performed the experiment and analyzed the data. K. F. supervised the project. All authors contributed to the writing of the paper.

[1] W. K. Wootters and W. H. Zurek, A single quantum cannot be cloned, Nature (London) **299**, 802 (1982).
[2] Charles H Bennett, Gilles Brassard, Claude Crépeau, Richard Jozsa, Asher Peres, and William K. Wootters, Teleporting an unknown quantum state via dual classical and Einstein-Podolsky-Rosen channels, Phys. Rev. Lett. **70**, 1895 (1993).
[3] Jian-Wei Pan, Dik Bouwmeester, Harald Weinfurter, and Anton Zeilinger, Experimental entanglement swapping: Entangling photons that never interacted, Phys. Rev. Lett. **80**, 3891 (1998).
[4] Stephanie Wehner, David Elkouss, and Ronald Hanson, Quantum internet: A vision for the road ahead, Science **362**, eaam9288 (2018).
[5] Koji Azuma, Sophia E. Economou, David Elkouss, Paul Hilaire, Liang Jiang, Hoi-Kwong Lo, and Ilan Tzitrin, Quantum repeaters: From quantum networks to the quantum internet, Rev. Mod. Phys. **95**, 045006 (2023).
[6] Dik Bouwmeester, Jian-Wei Pan, Klaus Mattle, Manfred Eibl, Harald Weinfurter, and Anton Zeilinger, Experimental quantum teleportation, Nature (London) **390**, 575 (1997).
[7] Ji-Gang Ren, Ping Xu, Hai-Lin Yong, Liang Zhang, Sheng-Kai Liao, Juan Yin, Wei-Yue Liu, Wen-Qi Cai, Meng Yang, Li Li *et al.*, Ground-to-satellite quantum teleportation, Nature (London) **549**, 70 (2017).
[8] Xiao-Min Hu, Yu Guo, Bi-Heng Liu, Chuan-Feng Li, and Guang-Can Guo, Progress in quantum teleportation, Nat. Rev. Phys. **5**, 339 (2023).
[9] Jian-Long Liu, Xi-Yu Luo, Yong Yu, Chao-Yang Wang, Bin Wang, Yi Hu, Jun Li, Ming-Yang Zheng, Bo Yao, Zi Yan *et al.*, Creation of memory–memory entanglement in a metropolitan quantum network, Nature (London) **629**, 579 (2024).
[10] C. M. Knaut, A. Suleymanzade, Y.-C. Wei, D. R. Assumpcao, P.-J. Stas, Y. Q. Huan, B. Machielse, E. N. Knall, M. Sutula, G. Baranes *et al.*, Entanglement of nanophotonic quantum memory nodes in a telecom network, Nature (London) **629**, 573 (2024).
[11] Pieter Kok and Samuel L. Braunstein, Postselected versus nonpostselected quantum teleportation using parametric down-conversion, Phys. Rev. A **61**, 042304 (2000).
[12] Jian-Wei Pan, Sara Gasparoni, Markus Aspelmeyer, Thomas Jennewein, and Anton Zeilinger, Experimental realization of freely propagating teleported qubits, Nature (London) **421**, 721 (2003).
[13] Nicolas Sangouard, Christoph Simon, Hugues De Riedmatten, and Nicolas Gisin, Quantum repeaters based on atomic ensembles and linear optics, Rev. Mod. Phys. **83**, 33 (2011).
[14] See Supplemental Material at http://link.aps.org/supplemental/10.1103/PhysRevLett.134.160802, which includes Ref. [15], for additional information about the experimental methods, data analysis, and theoretical modeling.

[15] Xiang Guo, Chang-ling Zou, Carsten Schuck, Hojoong Jung, Risheng Cheng, and Hong X Tang, Parametric down-conversion photon-pair source on a nanophotonic chip, Light Sci. Appl. **6**, e16249 (2017).
[16] Qi-Chao Sun, Ya-Li Mao, Si-Jing Chen, Wei Zhang, Yang-Fan Jiang, Yan-Bao Zhang, Wei-Jun Zhang, Shigehito Miki, Taro Yamashita, Hirotaka Terai *et al.*, Quantum teleportation with independent sources and prior entanglement distribution over a network, Nat. Photonics **10**, 671 (2016).
[17] Qi-Chao Sun, Yang-Fan Jiang, Ya-Li Mao, Li-Xing You, Wei Zhang, Wei-Jun Zhang, Xiao Jiang, Teng-Yun Chen, Hao Li, Yi-Dong Huang *et al.*, Entanglement swapping over 100 km optical fiber with independent entangled photon-pair sources, Optica **4**, 1214 (2017).
[18] Si Shen, Chenzhi Yuan, Zichang Zhang, Hao Yu, Ruiming Zhang, Chuanrong Yang, Hao Li, Zhen Wang, You Wang, Guangwei Deng *et al.*, Hertz-rate metropolitan quantum teleportation, Light Sci. Appl. **12**, 115 (2023).
[19] Nicolas Sangouard, Bruno Sanguinetti, Noé Curtz, Nicolas Gisin, Rob Thew, and Hugo Zbinden, Faithful entanglement swapping based on sum-frequency generation, Phys. Rev. Lett. **106**, 120403 (2011).
[20] Bereneice Sephton, Adam Vallés, Isaac Nape, Mitchell A. Cox, Fabian Steinlechner, Thomas Konrad, Juan P. Torres, Filippus S. Roux, and Andrew Forbes, Quantum transport of high-dimensional spatial information with a nonlinear detector, Nat. Commun. **14**, 8243 (2023).
[21] Xiaodong Qiu, Haoxu Guo, and Lixiang Chen, Remote transport of high-dimensional orbital angular momentum states and ghost images via spatial-mode-engineered frequency conversion, Nat. Commun. **14**, 8244 (2023).
[22] Yoon-Ho Kim, Sergei P. Kulik, and Yanhua Shih, Quantum teleportation of a polarization state with a complete Bell state measurement, Phys. Rev. Lett. **86**, 1370 (2001).
[23] Sebastien Tanzilli, Wolfgang Tittel, Matthaeus Halder, Olivier Alibart, Pascal Baldi, Nicolas Gisin, and Hugo Zbinden, A photonic quantum information interface, Nature (London) **437**, 116 (2005).
[24] Paul Fisher, Robert Cernansky, Ben Haylock, and Mirko Lobino, Single photon frequency conversion for frequency multiplexed quantum networks in the telecom band, Phys. Rev. Lett. **127**, 023602 (2021).
[25] Thiago Guerreiro, Enrico Pomarico, Bruno Sanguinetti, Nicolas Sangouard, J. S. Pelc, C. Langrock, M. M. Fejer, Hugo Zbinden, Robert T. Thew, and Nicolas Gisin, Interaction of independent single photons based on integrated nonlinear optics, Nat. Commun. **4**, 2324 (2013).
[26] Thiago Guerreiro, A. Martin, B. Sanguinetti, J. S. Pelc, C. Langrock, M. M. Fejer, N. Gisin, H. Zbinden, N. Sangouard, and R. T. Thew, Nonlinear interaction between single photons, Phys. Rev. Lett. **113**, 173601 (2014).
[27] Samuel L. Braunstein and Peter Van Loock, Quantum information with continuous variables, Rev. Mod. Phys. **77**, 513 (2005).
[28] Wolfgang Tittel, Jürgen Brendel, Hugo Zbinden, and Nicolas Gisin, Violation of Bell inequalities by photons more than 10 km apart, Phys. Rev. Lett. **81**, 3563 (1998).
[29] Norbert Lütkenhaus, John Calsamiglia, and K.-A. Suominen, Bell measurements for teleportation, Phys. Rev. A **59**, 3295 (1999).
[30] Fabian Ewert and Peter van Loock, 3/4-efficient Bell measurement with passive linear optics and unentangled ancillae, Phys. Rev. Lett. **113**, 140403 (2014).
[31] Matthias J. Bayerbach, Simone E. D'Aurelio, Peter van Loock, and Stefanie Barz, Bell-state measurement exceeding 50% success probability with linear optics, Sci. Adv. **9**, eadf4080 (2023).
[32] Mengdi Zhao and Kejie Fang, InGaP quantum nanophotonic integrated circuits with 1.5% nonlinearity-to-loss ratio, Optica **9**, 258 (2022).
[33] Hoi-Kwong Lo, Xiongfeng Ma, and Kai Chen, Decoy state quantum key distribution, Phys. Rev. Lett. **94**, 230504 (2005).
[34] Juan Miguel Arrazola and Norbert Lütkenhaus, Quantum fingerprinting with coherent states and a constant mean number of photons, Phys. Rev. A **89**, 062305 (2014).
[35] Félix Bussières, Christoph Clausen, Alexey Tiranov, Boris Korzh, Varun B. Verma, Sae Woo Nam, Francesco Marsili, Alban Ferrier, Philippe Goldner, Harald Herrmann *et al.*, Quantum teleportation from a telecom-wavelength photon to a solid-state quantum memory, Nat. Photonics **8**, 775 (2014).
[36] Hiroki Takesue, Shellee D. Dyer, Martin J. Stevens, Varun Verma, Richard P. Mirin, and Sae Woo Nam, Quantum teleportation over 100 km of fiber using highly efficient superconducting nanowire single-photon detectors, Optica **2**, 832 (2015).
[37] Raju Valivarthi, Marcel li Grimau Puigibert, Qiang Zhou, Gabriel H. Aguilar, Varun B. Verma, Francesco Marsili, Matthew D. Shaw, Sae Woo Nam, Daniel Oblak, and Wolfgang Tittel, Quantum teleportation across a metropolitan fibre network, Nat. Photonics **10**, 676 (2016).
[38] John F. Clauser and Michael A. Horne, Experimental consequences of objective local theories, Phys. Rev. D **10**, 526 (1974).
[39] Joseph B. Altepeter, Evan R. Jeffrey, and Paul G. Kwiat, Photonic state tomography, Adv. At. Mol. Opt. Phys. **52**, 105 (2005).
[40] Joshua Akin, Yunlei Zhao, Yuvraj Misra, A. K. M. Naziul Haque, and Kejie Fang, InGaP $\chi^{(2)}$ integrated photonics platform for broadband, ultra-efficient nonlinear conversion and entangled photon generation, Light Sci. Appl. **13**, 290 (2024).
[41] Dashiell L. P. Vitullo, M. G. Raymer, B. J. Smith, Michał Karpiński, L. Mejling, and Karsten Rottwitt, Entanglement swapping for generation of heralded time-frequency-entangled photon pairs, Phys. Rev. A **98**, 023836 (2018).

End Matter

Appendix A: SFG device—The $In_{0.5}Ga_{0.5}P$ microring resonator is phase-matched for two nondegenerate transverse-electric (TE_{00}) modes a and b in the telecommunication band and one transverse-magnetic (TM_{00}) mode c in the 780 nm band, satisfying the energy- and phase-matching conditions: $\omega_c = \omega_a + \omega_b$ and $m_c = m_a + m_b \pm 2$, where ω_k and m_k are the frequency and azimuthal number of mode k, respectively [14]. The three-wave-mixing interaction between these modes are described by the Hamiltonian $H/\hbar = g(a^\dagger b^\dagger c + abc^\dagger)$, where $a^\dagger(b^\dagger, c^\dagger)$ and $a(b, c)$ are the creation and annihilation operators of mode $a(b, c)$ and g is the single-photon nonlinear coupling rate. For the microring resonator used in this experiment, $\lambda_a = 1541.010$ nm, $\lambda_b = 1565.392$ nm, $\lambda_c = 776.553$ nm, and $g/2\pi \approx 14$ MHz. The linewidth of these resonances is approximately 4 GHz. The microring resonator is coupled with two bus waveguides for transmitting the 1550 nm and 780 nm band light separately, and these waveguides are combined at an on-chip wavelength-division multiplexer, allowing the use of a single optical fiber for coupling of all modes with a coupling efficiency of approximately 70% and 30% for the 1550 nm and 780 nm light, respectively. The device is mounted in a cryostat (4 K) to prevent wavelength drift of the nanophotonic cavity.

Appendix B: Non-postselected entanglement swapping—Consider entanglement swapping involving two nonlinear optics-based entangled photon sources, e.g., spontaneous parametric down-conversion sources, with single-pair generation probability $p_{A,si}$ and $p_{B,si}$, respectively. To gain some insight of the LO-BSM approach, first consider only the leading-order events with two input photons and lossless channels from the sources to the detectors. The fidelity of non-postselected entanglement swapping, i.e., without detection of the swapped photons, is given by

$$\mathcal{F} = \frac{p_{A,si}p_{B,si}}{p_{A,si}p_{B,si} + p_{A,si}^2 + p_{B,si}^2} \leq \frac{1}{3}, \tag{B1}$$

where the infidelity is attributed to two-pair emission events from the same source. The maximum fidelity of $\frac{1}{3}$ is achieved when $p_{A,si} = p_{B,si}$. This indicates that the fidelity of non-postselected entanglement swapping involving probabilistic sources via LO-BSM cannot be high because of the multiphoton emission.

If the loss of the two input channels of the LO-BSM is $\eta < 1$, as in long-distance optical-fiber networks, the optimal fidelity of non-postselected entanglement swapping can be rigorously calculated ([14]) and is given by

$$\mathcal{F} = \frac{1}{3}\left(\frac{1+\sqrt{1-4p_{si}}}{2}\right)^4, \tag{B2}$$

which is achieved when $p_{A,si} = p_{B,si} = p_{si}$. This result includes contributions of arbitrary multiphoton emission events from both sources but with only two photons detected overall, considering $\eta \ll 1$. The loss does not appear in Eq. (B2) because in all cases—one detected photon from each source or two detected photons from one source—the loss contributes a factor of η^2 for all terms. The optimal fidelity as a function of p_{si} is illustrated by the green curve in Fig. 5.

If the loss of the two input channels of the LO-BSM is unbalanced, e.g., $\eta \ll 1$ for one channel (from source B) and $\eta = 1$ for the other channel (from source A) for simplicity, which, for example, corresponds to the satellite-mediated entanglement swapping [i.e., a satellite (source B) emits entangled photons to two ground nodes that cannot be connected by optical fibers], the optimal fidelity of non-postselected entanglement swapping is given by ([14])

$$\mathcal{F} = \frac{1}{3}\left(\frac{1+\sqrt{1-4p_{B,si}}}{2}\right)^2, \tag{B3}$$

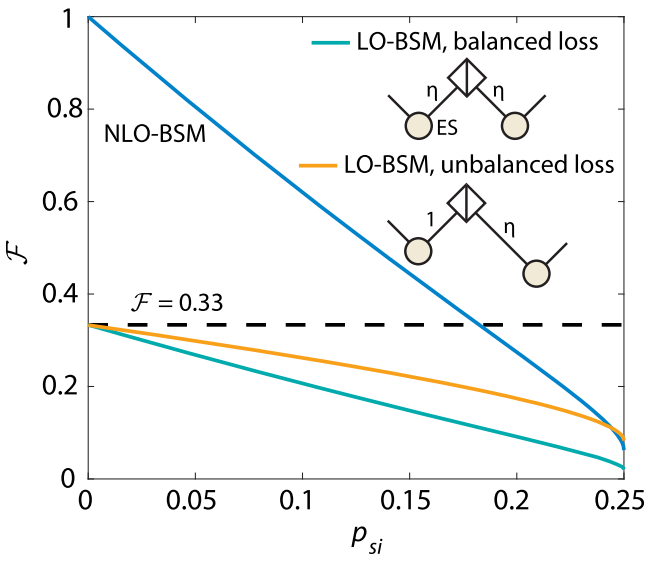

FIG. 5. Optimal fidelity of non-postselected entanglement swapping. Green: LO-BSM with balanced loss ($\eta \ll 1$) for two input channels. Yellow: LO-BSM with unbalanced loss. Dashed line indicates the bound $\mathcal{F} = 1/3$ for LO-BSM generally. Blue: NLO-BSM, which applies to both cases and the lossless case. Nonlinear optics-based entanglement source (ES) is assumed. For the blue and green curves, p_{si} is the single-pair generation probability of the two ESs. For the yellow curve, p_{si} is the single-pair generation probability of the ES in the lossy channel and that of the ES in the lossless channel is ηp_{si} for optimal fidelity. See Ref. [14].

which is achieved when $p_{A,si} \approx \eta p_{B,si}$. This result includes contributions of arbitrary multiphoton emission events from source B and zero-, one-, and two-photon emissions from source A, with two photons detected overall. This shows that, in the loss-unbalanced case, the entangled photon source with less loss needs to be attenuated to prevent its multiphoton emissions from degrading the fidelity. The optimal fidelity as a function of $p_{si} = p_{B,si}$ is illustrated by the yellow curve in Fig. 5. Although the loss does not affect the optimal fidelity given by Eqs. (B2) and (B3) when $\eta \ll 1$, it does of course affect the success probability, which scales as η^2, in both cases.

The fidelity of non-postselected entanglement swapping can be significantly enhanced by using NLO-BSM, which is given by ([14]):

$$\mathcal{F} = \left(\frac{1+\sqrt{1-4p_{A,si}}}{2}\right)^2 \left(\frac{1+\sqrt{1-4p_{B,si}}}{2}\right)^2. \quad \text{(B4)}$$

This result holds for both the lossless case and the two lossy cases above. The fidelity as a function of $p_{si}(= p_{A,si} = p_{B,si})$ is illustrated by the blue curve in Fig. 5. In addition to the fidelity advantage, the NLO-BSM approach can actually be more efficient than the LO-BSM approach in some cases, including the loss-unbalanced case. In particular, the entanglement rate for LO-BSM in this case is given by

$$R_{\mathrm{LO}} = p_{A,si}\eta p_{B,si} R_c = \eta^2 p_{B,si}^2 R_c, \quad \text{(B5)}$$

where we have used $p_{A,si} = \eta p_{B,si}$ for the optimal fidelity and R_c is the clock rate. In contrast, the entanglement rate for NLO-BSM is given by

$$R_{\mathrm{NLO}} = p_{\mathrm{SFG}} p_{A,si}\eta p_{B,si} R_c = p_{\mathrm{SFG}}\eta p_{B,si}^2 R_c, \quad \text{(B6)}$$

where $p_{A,si}$ can be as large as $p_{B,si}$. When $p_{\mathrm{SFG}} > \eta$, the NLO-BSM approach can be more efficient than the LO-BSM approach. This is relevant, for example, for satellite-mediated entanglement swapping, given the available $p_{\mathrm{SFG}} = 10^{-4}$–$10^{-3}$ using our nanophotonics platform while the loss of satellite-ground link can be > 50 dB [7].